Above threshold photodissociation in H2 and H2+

A. Bandrauk, E. Constant, J.-M. Gauthier

Classification
Physics Abstracts
33.80G — 33 80W — 42.50

Above threshold photodissociation in H_2 and H_2^+

A D Bandrauk, E Constant (*) and J.-M. Gauthier

Département de chimie, Faculté des sciences, Université de Sherbrooke, Sherbrooke, Québec, J1K 2R1, Canada

(*Received 12 March 1991, accepted in final form 27 May 1991*)

Abstract. — A coupled equations approach is used to calculate the probabilities of photophysical processes in the *ten* photon absorption spectrum of H_2 at wavelength $\lambda = 532$ nm At high intensities, i e , $I > 10^{10}$ W/cm^2, it is shown that *above threshold photodissociation* (ATPD) occurs readily in the B $^1\Sigma_u^+$ state of H_2 and in X $^2\Sigma_g^+$ of H_2^+ Laser-induced avoided crossings between the dressed *B* and *F* electronic potentials of H_2 and also between the dressed *X* and *A* potentials of H_2^+ result in anomalous proton yields at intensities above 10^{11} W/cm^2. The vibronic structure of the dressed X $^2\Sigma_g^+$ potential of H_2^+ appears in all photodissociation yields as laser-induced resonances with intensity dependent line widths

1. Introduction.

Great progress in our understanding of the electronic structure of molecules has come from the introduction of the molecular orbital concept by Mulliken in the 1950's and 60's. Thus as in atoms, electrons in molecules occupy orbitals which envelope the whole nuclear space, creating stable molecular species if the molecular orbitals are bonding and unstable species if these are antibonding [1]. The bonding characteristics of molecular orbitals can be inferred from photoelectron spectroscopy [2]. Recent improvements in this method has even led to determination of the electron momentum distribution in these orbitals [3]. A concomitant structure which appears often in the photo electron spectrum is the vibronic structure of the remaining molecular ion after photoionization This structure which is created by the coupling of the ionized electron to the core of the ion reveals the vibrational structure of the molecular ion and the degree of coupling between both electron and ion [4] We conclude therefore that the electron serves as an essential probe in understanding molecular structure

The advent of intense lasers has revealed some singular aspects of the nonlinear behaviour of atoms in intense laser fields [5-7] Recently, similar nonlinear phenomena (e g , above threshold ionization, ATI), have been observed in molecules [8-11] In particular, experiments on the nonlinear photoionization of H_2 have revealed that the vibronic structure of the molecular ion is considerably altered with respect to the free ion [9, 10] It is the goal of this

(*) Département de Physique, Université de Reims.

work to present new results based on a theoretical model, the *dressed molecule,* which can help us understand nonlinear molecule-laser interactions, which interactions we reiterate are induced by multiphoton transitions (real and virtual) of the electrons in the molecule.

One can classify the regime of coupling between the laser and the molecular system according to the nature of the process they induce. The first regime is that corresponding to low-intensity lasers which couple weakly with the system. As a result, the excitation processes are well described by leading order perturbation theory, such as Fermi's Golden rule. For molecules, this leads to a Franck-Condon picture of electronic (radiative) transitions [12]. At intermediate to high intensities, one encounters a domain in which multiphoton processes begin to take effect. This is signalled by nonlinear behaviour of the transition probabilities as a function of intensity. In particular two or more states may be strongly coupled together as a result of being near resonant. An example of this is the Rabi oscillations of a two level atom [5, 6] or an *n*-level molecule [13]. Another example which this chapter discusses in detail, is the nonlinear interaction between vibrational manifolds of different electronic molecular states induced by intense laser fields Judging from atomic experience, [14], one can establish the upper limit of the intensity I of this regime at 10^2 W/cm^2 (tera-watt/cm^2), since for $I > 10^{13}$ W/cm^2, ionization rates exceed dissociation rates for many molecules. Finally one has the very high intensity limit available with current superintense lasers ($I > 10^{13}$ W/cm^2), where Rabi frequencies ($\omega_R = d\mathcal{E}/\hbar$, d = transition moment, $\mathcal{E}$= electric field) are comparable to the laser frequency, and highly nonresonant transitions compete with resonant processes Thus in the case of the nonlinear photoelectron spectroscopy of H_2 mentioned above [8-11], the photoionized electron continues to absorb photons creating ATI peaks with a vibronic structure which has no relation to the vibrational structure of free H_2^+. We will show that the H_2^+ core is dressed by the intense field and that the vibrational structure of the photodissociation peaks reflects the nonlinear interaction of the ion core with the laser while at the same time remaining coupled to the dressed photoionized electron.

In particular we will show that intense lasers can create dressed *adiabatic* states as a result of a laser induced avoided crossing between the ground bonding state X^+ ($^2\Sigma_g^+$) of H_2^+ and the dissociative antibonding state A^+ ($^2\Sigma_u^+$) of that ion From a semiclassical analysis of the problem [15, 16], one can predict a *stabilization* of new dressed molecular states. This stabilization stems from the molecule resonating between the two bound states, diabatic (unperturbed) and adiabatic (perturbed) of the molecule Such stabilization of electronic states at high intensities is currently being discussed extensively in the atomic case [17, 18]. In the molecular case, the nuclear degrees of freedom offer the possibility of creating stable new electronic states by the laser induced coherent superposition of bonding and antibonding states of the free molecule In the following, we will show the realization of this effect within a more realistic close-coupling calculation involving many electronic-field states, as befits such a highly nonperturbative problem. We also point out that at high intensities, where Rabi frequencies exceed rotational spacings, laser-induced orientational effects or alignment are expected to predominate in the angular distribution of photodissociation fragments [19].

2. Theoretical method. Coupled equations.

We shall elaborate in the present section on the coupled equations in the field-molecular representation which leads to a proper and accurate description of dressed molecular states at high intensities [15, 16, 19, 20].

For the present, let us consider the general case of photodissociation of a simple diatomic. The Hamiltonian for the system may be partitioned into four components, namely,

$$\hat{H} = \hat{H}_m + \hat{H}_{na} + \hat{H}_f + \hat{H}_{mf}, \tag{1}$$

in which the molecular interactions are denoted by $\hat{H}_m$, the Hamiltonian of the Born-Oppenheimer approximation, and $\hat{H}_{na}$, the nonadiabatic perturbation. The quantized radiation fields are defined in [21-24] and are represented by the term

$$\hat{H}_f = \sum_k \omega_k \hat{a}_k^+ \hat{a}_k , \tag{2}$$

in which the summation is over the frequencies ω_k and wave vector k of the modes The creation and annihilation operators $(\hat{a}_k^+, \hat{a}_k)$ have their usual meaning, i.e., creation of a photon in emission, annihilation in absorption. Lastly the radiative interaction between the molecules and the fields is denoted by the term $\hat{H}_{mf}$ and takes the form in the quantized field representation and dipole approximation [5, 6, 25],

$$\hat{H}_{mf} = \mathbf{d} \cdot \boldsymbol{\mathcal{E}} = \sum_k \left(\frac{2\pi\omega}{L} k \right)^{1/2} \mathbf{e}^{(k)} \cdot \mathbf{d}^{(k)} (\hat{a}_k + \hat{a}_k^+) , \tag{3}$$

in which $\mathbf{e}$ denotes the polarization vector, L is the size of the cavity, and $d^{(k)}$ designates the dipole moment of the molecule for the k^{th} transition. The effect of nonadiabaticity can be treated simultaneously and can play an important role as in the multiphoton infrared dissociation of ionic molecules [26].

A measure of the various interstate couplings involved will help in understanding the dynamics Radiative couplings can usually be expressed as a Rabi frequency

$$\omega_R(\text{cm}^{-1}) = \mathbf{d} \cdot \boldsymbol{\mathcal{E}}/\hbar = 1.17 \times 10^{-3} \, d \, (\text{a.u.}) \, I \, [\text{W/cm}^2]^{1/2} , \tag{4}$$

$$I = \frac{8\pi}{c} \mathcal{E}_0^2 , \tag{5}$$

where a u. denotes atomic units, c is the velocity of light, the intensity I is reported in watts/cm^2 and $\mathcal{E}_0$ is the maximum field amplitude. For a dipole transition moment $d \sim 1$ a.u., and an intensity $I = 10^{11}$ W/cm^2, one obtains a radiative interaction of ~ 400 cm^{-1}. This is to be compared with the nonradiative (nonadiabatic) interaction between the covalent and ionic state of LiF, $\langle \psi(\text{LiF}) | \, H_{el} \, | \psi(\text{Li}^+ \, \text{F}^-) \rangle \simeq 600$ cm^{-1}, as an example [26] whereas the vibrational frequency of LiF is ω (LiF) = 300 cm^{-1}. It is clear that at high intensities ($I > 10^{10}$ W/cm^2), radiative interactions are *nonperturbative* and will compete with the nonradiative interactions, hence influencing considerably the photodissociation ratios of branching into various product excited atomic states.

We will endeavour to show in this section that the model of the dressed molecule and the Born-Oppenheimer approximation [1, 12], lead to the determination of the dressed or field-molecule eigenstates as solutions to coupled differential equations that describe the nuclear motion in the presence of the laser field Thus bound-discrete, bound-continuum, radiative and nonradiative (nonadiabatic) can all be treated simultaneously for any coupling strength, thus allowing us to go beyond the usual perturbative treatments Since we shall be dealing with bound states as *initial* conditions, the presence of dissociative (continuum) nuclear states presents a problem, which is circumvented through the use of a scattering formalism that encompasses all possibilities Thus, by introducing the technique of artificial channels for entrance [27] and generalized to include exit channels also [7, 20], one can simultaneously treat bound and continuum states. It is thus possible by the present method to calculate rigorously *transition amplitudes* for any radiative or nonradiative interaction strength in the presence of bound and continuum states, thus covering both perturbative (Fermi-Golden rule) and nonperturbative regimes.

We rewrite the total Hamiltonian (1) by separating the radiative and nonradiative perturbation, $\hat{H}_{mf}$ and $\hat{H}_{na}$,

$$\hat{H} = \hat{H}_0 + \hat{V}\,; \quad \hat{H}_0 = \hat{H}_m + \hat{H}_f\,, \quad \hat{V} = \hat{H}_{mf} + \hat{H}_{na} \tag{6}$$

Thus $\hat{H}_0$ is the zeroth-order field-molecule Hamiltonian, and $\hat{V}$ is the total, radiative and nonradiative interaction. We now try to express the field molecule eigenstates of the total Hamiltonian in terms of the eigenstates of $\hat{H}_0$, which are therefore direct products of the unperturbed (Born-Oppenheimer) molecular eigenstates of $\hat{H}_m$, and the unperturbed field eigenstates of $\hat{H}_f$, equation (2) We can therefore define the *field-electronic* states

$$|e, n\rangle = |e\rangle\,|n\rangle\,, \tag{7}$$

where e is a collective quantum number (symmetry, spin, etc.) for molecular Born-Oppenheimer electronic states, and n is the photon number We now look for solutions of the total Schrödinger equation : $\hat{H}|\psi_E\rangle = E|\psi_E\rangle$ with the total wave function expanded in terms of the basic field-electronic states defined in (7),

$$|\psi_E\rangle = \frac{1}{R}\sum_{e,n} F_{en}(R)\,|e, n\rangle \tag{8}$$

$F_{en}(R)$'s are appropriate nuclear radial functions propagating on the potential of the photon-electronic state $|e, n\rangle$ By substituting into the total Hamiltonian defined in equation (6), and premultiplying by a particular state $|e, n\rangle$, one obtains the set of one-dimensional second-order differential equations for $F_{en}(R)$:

$$\left\{\frac{d^2}{dR^2} + \frac{2m}{\hbar^2}\,[E - V_e(R) - n\hbar\omega\,]\right\} F_{en}(R) = \frac{2m}{\hbar^2}\sum_{e'n'} V_{en,e'n'}(R)\,F_{e'n'}(R)\,, \tag{9}$$

where m is the reduced mass of the molecule, $V_e(R)$ is the field free electronic potential of electronic state $|e\rangle$ obtained from *ab-initio* quantum chemical calculations or from spectroscopic measurements [1, 12]. We treat here rotationless molecules, although in principle both rotational quantum numbers (J, M) can be included rigorously [19, 27].

Equation (9) for the field-molecule problem can be more succinctly expressed in matrix form as,

$$F''(R) + W(R)\,F(R) = 0\,, \tag{10}$$

where the diagonal energy matrix elements are

$$W_{en,en}(R) = \frac{2m}{\hbar^2}\,[E - V_e(R) - n\hbar\omega\,]\,. \tag{11}$$

The nondiagonal elements that describe the couplings, i.e.,

$$W_{en,e'n'}(R) = \frac{2m}{\hbar^2}\,[V^m_{en,e'n}(R) + V^r_{en,e',n\pm1}\,]\,, \tag{12}$$

are of two types : nonradiative ($\hat{V}^m = \hat{H}_{na}$) and radiative ($\hat{V}^r = \hat{H}_{mf}$). Since each electronic potential $V_e(R)$ appears in the diagonal matrix elements (11), we are able to sum numerically

over all bound vibrational and continuum (unbound) states of the same potential. Thus only the electronic and photon states need be specified explicitly in any numerical calculation. Finally the radiative couplings $\hat{V}^r$ are nondiagonal in the photon quantum numbers reflecting annihilation (absorption, $\Delta n = -1$) or creation (emission, $\Delta n = +1$) of a photon. The nonradiative (nonadiabatic) couplings V^m remain diagonal in the photon number n since they do not involve the field.

All numerical calculations are performed using a Fox-Goodwin method, which has proved to be very accurate for molecular problems (errors are of sixth order in the integration step [28]). The asymptotic numerical radial functions are projected onto asymptotic field-molecule states $|e, n\rangle$ and are expressed as,

$$F_{en}(R) = \sum_{e'n'} F_{en}^{e'n'}(R),$$

$$F_{en}^{e'n'}(R) = k_{en}^{-1/2}\{\delta_{ee'}\,\delta_{nn'}\exp[-\imath(k_e R + \delta)] - S_{en,e'n'}\exp[\imath(k_{e'} R + \delta)]\}, \qquad (13)$$

$$k_{en}^2 = \frac{2m}{\hbar^2}(E - V_e(R_\infty) - n\hbar\omega)$$

δ is an elastic scattering phase factor, which is zero for neutral dissociating products but needs to be modified for charged products [26].

The coefficients $S_{en,e'n'}$ are defined as the scattering, S-matrix elements, and the function $F_{en}^{e'n'}(R)$ corresponds to the nuclear radial functions of the molecule in the final state $|e, n\rangle$ for initial states $|e', n'\rangle$. In practice one usually projects the real numerical functions onto real asymptotic states, i.e.,

$$F_{en}^{e'n'}(R) = k_e^{-1/2}[\delta_{ee'}\,\delta_{nn'}\sin(k_e R + \delta) + R_{en,e'n'}\cos(k_e R + \delta)]. \qquad (14)$$

This projection enables one to obtain, from the numerical procedure, the R matrix, which is related to the S matrix by the expression [29]

$$S = (1 - \imath R)^{-1}(1 + iR), \qquad (15)$$

and thus one obtains the transition amplitude matrix T,

$$S = 1 - 2\pi\imath T. \qquad (16)$$

In the molecular problems we shall encounter, invariably the initial state is a bound state, so that one encounters the problem of bound-bound transitions, or one has to calculate the probability of transition from initial bound states to final continuum photodissociation states. In one method, such as encountered in the complex-coordinate method [30], one calculates linewidths Γ directly from the imaginary part of the energy. We have shown previously [19-20, 27], that it is possible to obtain transition amplitudes directly from the coupled equations (10), i.e., one can transform all transition amplitude problems, including bound-bound transitions, into a scattering problem by introducing additional *artificial* channels, continua, as entrance and exit channels. The introduction of such artificial channels (first suggested by Shapiro for direct photodissociation amplitude calculations ([31]) into the coupled equations (10) permits us to exploit the various relations between transition matrices in order to extract the relevant photophysical amplitudes. Thus using the following relations between the total Green's function G and the transition operator T [32, 33],

$$T = V + VG_0\,T = V + TG_0\,V, \qquad (17)$$

$$G = G_0 + G_0 TG_0\,, \quad G = (E - H)^{-1}\,, \quad G_0 = (E - H_0)^{-1}\,, \tag{18}$$

one can obtain an expression for the transition amplitude T_{CCl} between an entrance channel $|C1\rangle$ and a real physical continuum (dissociative) channel $|c\rangle$,

$$T_{C1,C} = \exp(i\eta_1)\, V_{C1,0}\, G_0^0\, T_{0C}\,. \tag{19}$$

G_0^0 is the zeroth order (field-molecule) Green's function of the initial bound state $|0\rangle$, η_1 is the elastic phase shift for scattering on the artificial continuum potentials of $|C1\rangle$, and $C_{C1,0}$ is the coupling (weak) between the artificial channel and the bound state. The numerical solutions of the coupled equations (9)-(10) including the artificial channel $|C1\rangle$ coupled to the initial state with n photons $|0, n\rangle$ permits us to extract each photodissociation amplitude

$$T_{0C} = T_{C1,C} \exp(-i\eta_1)(V_{C1,0}\, G_0^0)^{-1} \tag{20}$$

All quantities on the right hand side of equation (20) can be calculated numerically [19, 20]. The above method applies provided the initial state $|0\rangle$ is only weakly perturbed during the multiphoton processes, so that the unperturbed Green's function G_0^0 is adequate. This will be the case if the initial state is coupled nonresonantly to resonant processes, as will be shown to occur in the H_2 case (next section). All multiphoton resonant processes and nonadiabatic interactions are calculated exactly in T_{0C}, allowing us to join the weak, perturbative regime ($I < 10^{10}$ W/cm^2) to the strong, nonperturbative regime ($I > 10^{10}$ W/cm^2).

3. The dressed molecule.

Having established in the previous section the necessary formalism to treat multiphoton transitions in diatomic molecules beyond perturbation theory, we now expose in detail the method in order to help interpret the recent experimental results of van Linden van den Heuvell [9] and Bucksbaum [10] on the nonlinear photoelectron spectrum of H_2 which exhibits above threshold ionization peaks (ATI), i.e., the ionized electron keeps absorbing photons in the vicinity of the molecular ion core. Each ATI peak now reveals a vibronic structure, as the receding electron remains coupled to the core *via* Coulomb and polarization forces. Furthermore, measurements by Bucksbaum *et al* [10] on the proton yield demonstrate unusual yield dependencies on the intensity of the laser.

We limit ourselves in the present work to the experimental laser wavelength $\lambda = 532$ nm As pointed out by van Linden van den Heuvell [9], this wavelength allows one to reach the $B\,^1\Sigma_u^+$ state of H_2 *via* a five photon *nonresonant* transition (see Fig 1). A sixth photon couples radiatively and resonantly the B state to the doubly excited $2p\sigma_u^2$ electronic state, the so called F state which crosses in a *diabatic* representation [33] the Rydberg type E electronic state [12]. In an adiabatic representation, the EF curve forms a double well as does the GK potential. These two states remain coupled by a nonadiabatic (non Born-Oppenheimer) coupling. One can however adopt the equivalent diabatic representation where now the diabatic GF and EK curves cross (Fig. 1) and are coupled by a nonradiative *nondiabatic* coupling due to the fact that in this representation the molecular electronic Hamiltonian $\hat{H}_m$ is not diagonal. A residual nondiabatic coupling $\langle EK|\,\hat{H}_{el}\,|GF\rangle$, the term $\hat{H}_{na}$ in the Hamiltonian (6) is operative. In fact the diabatic EK and GF electronic potentials were obtained by deperturbing with a 2×2 unitary transformation the spectroscopic adiabatic electronic states EF and GK (for details see [12, 34]) This procedure yields a nondiabatic coupling $\hat{H}_{na}(R)$ which is used in the coupled equations (9). It is to be emphasized once more

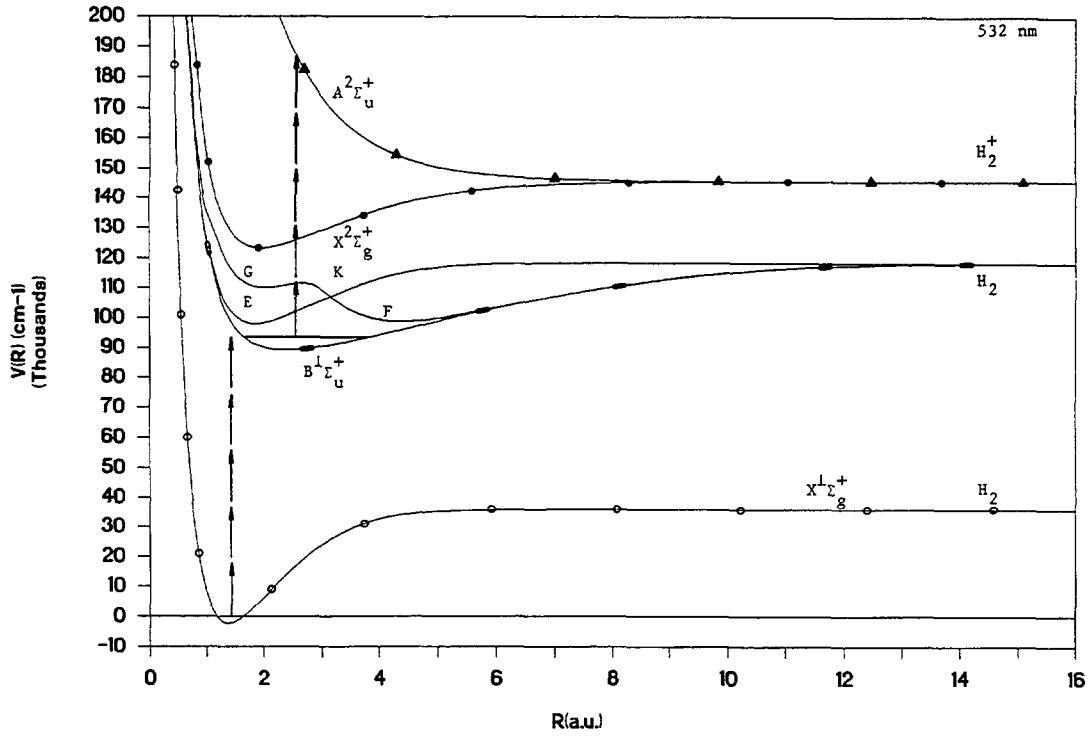

Fig 1 — Ten photon absorption in H_2 at $\lambda = 532$ nm leading to dissociation of H_2^+ EK and GF states are diabatic electronic potentials of H_2. (O) $X(H_2)$, (—) $B(H_2)$, (•) $X^+(H_2^+)$, (▲) $A^+(H_2^+)$

that in the coupled equations formalism, both non-diabatic (we now use this term in a diabatic representation rather than nonadiabatic which applies to an adiabatic regime) interstate couplings and radiative couplings are equivalent from a formal view point. The numerical procedure presented in the previous section allows for the rigorous treatment of radiative and nonradiative transitions on an equal footing, from the perturbative (weak interaction) limit to the nonperturbative (strong interaction) limit

The sixth photon is thus resonant with the vibrational states of the GK and EK diabatic electronic potentials which further interact nondiabatically. A seventh photon now couples radiatively these last states to the X^+ ($^2\Sigma_g^+$) ground electronic state of H_2^+ In this process, a free electron is now created so that the electronic transition moment involves the Rydberg electrons of the E and G states and the ionizing electron in H_2^+ (assuming that the H_2^+ core is nearly the same for the E, G and X^+ states (see Fig 1)). We emphasize that the F state, which is doubly excited *cannot* couple radiatively directly to the X^+ state, i.e, the electronic transition moment $\langle 2p\sigma_u^2 | \mathbf{r} | 1s\sigma_g f_c \rangle$, where f_c is the ionized electron wavefunction is rigorously zero since radiative transitions, if one neglects electron correlation, involve only one electron excitation [12]. We thus have the interesting case that the B state couples *radiatively* strongly to the F state, which then couples *nonradiatively* to the Rydberg E and G states. It is from these two Rydberg states that the seventh photon of wavelength 532 nm can now access resonantly the H_2^+ molecule, leading to ATI when the ionized electron keep absorbing further photons. This last process leads to dressing of the electron and various theoretical methods have been developed over the years to treat this problem [5-6], albeit for atoms only so far.

What we wish to point out is that in the course of ATI, a purely electronic process as a first approximation, photons will interact further with the H_2^+ core leading to a dressing of the H_2^+ molecular ion Firstly, a nonresonant three photon transition induces direct photodissociation from the bound $X^+ (^2\Sigma_g^+)$ state to the repulsive, dissociative $A^+ (^2\Sigma_u^+)$ of H_2^+ This is seen in figure 1, the standard nonperturbative vertical image of multiphoton transitions. The more complete nonperturbative representation is that of figure 2 where we now use the field-molecule states defined in the previous section, equations (7)-(8) (i.e., the total wavefunction is linear superposition of products of photon and molecular states). Let us now explain in detail the meaning of this new representation. The ground $X(^1\Sigma_g^+)$ state with $(n + 5)$ photons couples radiatively nonresonantly to the $B(^1\Sigma_u^+)$ state leaving only n photons after a five photon transition. Since this transition is *nonresonant,* it will be weak and can be treated perturbatively. The remaining transitions, being *resonant,* are strong and must be treated nonperturbatively. Thus the $B(n)$ state is coupled radiatively to two sets of states : the $GF(n - 1)$ and $GF(n + 1)$ field-molecule states The first $(n - 1)$ state corresponds to removal of one photon from the field and is thus ascribed to an *absorption.* The second

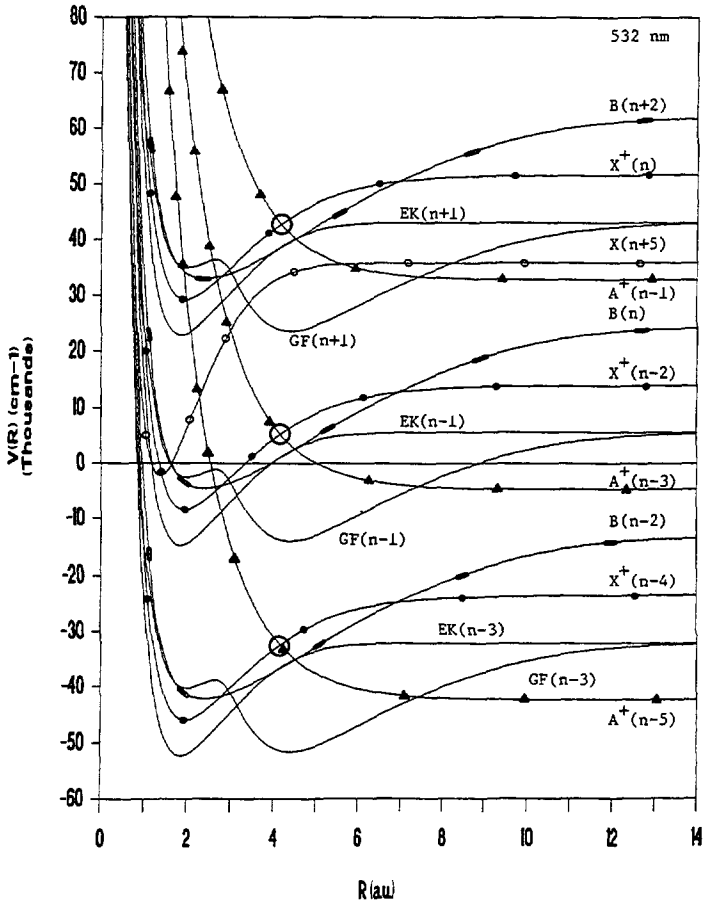

Fig 2 — Field-molecule (dressed) representation of figure 1 with photon numbers n All channels below zero energy line are open (physical) All channels above zero are closed, giving rise to laser-induced resonance structures (O) Laser induced avoided crossings. (O) $X(H_2)$; (—) $B(H_2)$; (•) $X^+ (H_2^+)$; (▲) $A^+ (H_2^+)$.

$(n+1)$ state is the result of a *virtual* photon emission We remind the reader that the quantized electric field, equations (2)-(3) is explicitly written as the sum of an annihilation ($\hat{a}$) and a creation ($\hat{a}^+$) photon operator. The first corresponds to absorption and the second to emission of photons We must emphasize that at 532 nm wavelength the B → F transition is resonant for absorption. Thus the GF$(n-1)$ state crosses resonantly the B(n) state in the Franck-Condon region for that transition. The B(n) → GF$(n+1)$ transition is nonresonant and is therefore called a *virtual* transition (this transition is responsible for the Lamb shift of electronic states in vacuum [21-24]). In the field-molecule picture one sees immediately, figure 2, that this transition is nonresonant. In fact the GF$(n+1)$ state is $2\hbar\omega$ in energy above the resonant B → F transition. This point helps us establish the validity of the rotating wave approximation, RWA, which neglects all such virtual transitions [5-6]. This approximation is therefore valid only if the Rabi frequency, ω_R (Eq. (4)), the radiative coupling between the B and F state is much less than the energy separation between the resonant and the virtual transition, i.e. $\omega_R \ll 2\hbar\omega$. This is the main reason why in the X → B five photon transition, only the X$(n+5)$ and B(n) field molecule states are used The virtual coupling between the X$(n+5)$ and B(n') states, where $n' > n$ can be safely neglected since the photon absorptions are themselves nonresonant, and are therefore very weak. In conclusion, every resonant $n \to n-1$ absorption is accompanied by a virtual $n \to n+1$ emission This explains therefore the doubling of all electronic states in figure 2

We now continue to follow the photon paths. The GF states are coupled nondiabatically (*via* $\hat{H}_{na}$, i.e , $V^m_{en,e'n}$ Eq. (12)), to the EK states with the same photon number since this is a *nonradiative* transition. Now the Rydberg E and G$(n-1)$ states couple resonantly to the $X^+(n-2)$ and virtually to $X^+(n)$ state of H_2^+. The $X^+(n-2)$ state couples nonresonantly to the $A^+(n-3)$ and virtually to the $A^+(n-1)$ state The $A^+(n-3)$ state couples radiatively to $X^+(n-4)$ and $X^+(n-2)$ The first transition corresponds to the nonresonant absorption of the *ninth* photon shown in figure 2. The virtual transition $A^+(n-3) \to X^+(n-2)$ serves to dress the X^+ electronic state, and is depicted in figure 3. Thus the $X^+(n-2)$ and $A^+(n-3)$ field-molecule states cross at an energy above the $v=4$ vibrational level of the X^+ ground state of H_2^+. The symmetric radiative coupling $\langle X^+ | \boldsymbol{\mu} | A^+ \rangle \boldsymbol{\mathcal{E}}$ gives rise to both the absorption $X^+(n-2) \to A^+(n-3)$ and the emission $A^+(n-3) \to X^+(n-2)$ processes. Similar crossings occur in the other field-molecule states which must be added until numerical convergence is achieved. We repeat, this is due to the fact that the classical coherent electric field $\mathcal{E}$ is a linear superposition of photon states n [21-24] Finally we have a transition from the $X^+(n-4)$ to the $A^+(n-5)$ state. This last state corresponds to the photodissociation-ionization of $H_2(X\,^1\Sigma_g^+)$ to $H_2^+(A\,^2\Sigma_u^+)$ after absorption of ten photons, or the three photon photodissociation of H_2^+

The figure 2 represents the minimal number of field-molecule states required for a proper treatment of the nonlinear photoelectron spectrum of H_2. As the intensity increases, more and more of those states must be included until numerical convergence is achieved. In the weak field limit, one recovers of course the direct perturbative pathway described by figure 1. In the strong field limit, many more pathways are allowed due to the virtual photon creation processes which are normally neglected in the RWA regime Thus the complete state count as exhibited in figure 2 allows us to bridge the weak and strong field limits

The field-molecule representation depicted in figure 2 leads us to make the following quick predictions. Firstly, crossings of field-molecular states involving a one photon resonant process become *laser-induced avoided crossings* as one increases the field intensity I. Thus the crossings of the states $X^+(n)$, $A^+(n-1)$, $X^+(n-2)$, $A^+(n-3)$, $X^+(n-4)$, $A^+(n-5)$ all undergo an avoided crossing as shown in figure 3 for various laser intensities The new field-molecule states are obtained by diagonalizing the diabatic 2×2 Hamiltonian (in a first

resonant approximation)

$$H_d = \begin{pmatrix} V_{11}(R) + \hbar\omega & V_{12}(R) \\ V_{21}(R) & V_{22}(R) \end{pmatrix}, \quad (21)$$

giving two new *adiabatic* states, called the *dressed* states of the field-molecule system :

$$V_{\pm}(R) = \frac{V_{11}(R) + V_{22}(R) + \hbar\omega}{2} \pm 1/2[(V_{11}(R) + \hbar\omega - V_{22}(R))^2 + 4\,V_{12}^2(R)]^{1/2}, \quad (22)$$

where V_{11}, V_{22} are the diabatic (zero-field) molecular electronic potentials (Fig. 1), V_{12} is the radiative coupling (Rabi frequency, Eq. (4)). Similar laser-induced avoided crossings occur at the intersections of the $B(n)$, $GF(n-1)$; $B(n+2)$, $GF(n+1)$; $B(n-2)$, $GF(n-3)$ states. These radiative avoided crossings are further perturbed by the nondiabatic interactions with the EK states. These laser induced avoided crossings induce nonperturbative intensity dependent changes in the electronic potential and concomitantly in the vibronic structure of transitions. Such laser induced effects have been considered by various authors [35-38, 15, 16]. A detailed study of laser induced resonances, i.e., the nonlinear radiative lifetimes of photodissociating molecular states such as shown in figure 3 has been undertaken by Bandrauk *et al.* [15-16]. In particular, a semiclassical approach used previously in the theory of *predissociation* of molecules has proven to be very useful in predicting the existence of these new resonances. This is in keeping with the remark made above that in the field-molecule representation, nondiabatic (nonradiative) and radiative interactions are formally equivalent and can be treated simultaneously in a unified formalism. The scattering formalism expounded in the previous section is of course the most convenient method to treat bound and continuum states simultaneously in the presence of large radiative and nonradiative interactions The experimental observation of a laser intensity dependent vibronic structure of H_2^+ was observed recently [9-10] and was therefore the first confirmation of the laser induced avoided effect illustrated in figure 3.

Figure 2 further demonstrates that at the wavelength of 532 nm five open channels appear, i.e. channels below the initial zero energy. These channels correspond to dissociation of H_2 and H_2^+ into neutral atoms and protons. Thus the $A^+(n-3)$, $X^+(n-4)$ and $A^+(n-5)$ channels will produce H(1s) and H^+ species with kinetic energies corresponding to the difference in energy between the zero line (energy of $v = 0$, $X\,^1\Sigma_g^+$ of H_2) (Fig. 2) and the asymptotic energies of each state. Hence three protons of different kinetic energy are to be expected. The lowest energy proton will emanate from the $A^+(n-3)$ channel as a result of the tunnelling of the vibrational states of $X^+(n-2)$ at the initial zero energy. A second higher energy photon will be produced by the $X^+(n-4)$ channel, which corresponds to the ninth proton process in figure 2, or equivalently the two photon dissociation of H_2^+ *via* the *nonresonant* process $X^+(n-2) \rightarrow A^+(n-3) \rightarrow X^+(n-4)$. Figure 2 tells us immediately that this final channel, $X^+(n-4)$ is coupled radiatively to $A^+(n-5)$, so that a laser-induced avoided crossing will occur between these two channels at the energy 32 000 cm^{-1} below the initial zero energy. Thus the yield of the first low energy proton from $A^+(n-3)$ and the second and third higher energy protons from $X^+(n-4)$ and $A^+(n-5)$ are all expected to be nonperturbatively influenced at high intensities by the laser-induced avoided crossings illustrated in figure 3. The high kinetic energy protons from $A^+(n-5)$ are the result of the three-photon nonresonant transition of H_2^+, the last three photons in figure 1. The field-molecule picture illustrates that this three-photon transition will be strongly affected by the two photon transition $X^+(n-2) \rightarrow X^+(n-4)$ at high intensities.

This two-photon transition merits further elaboration As indicated above, this is a

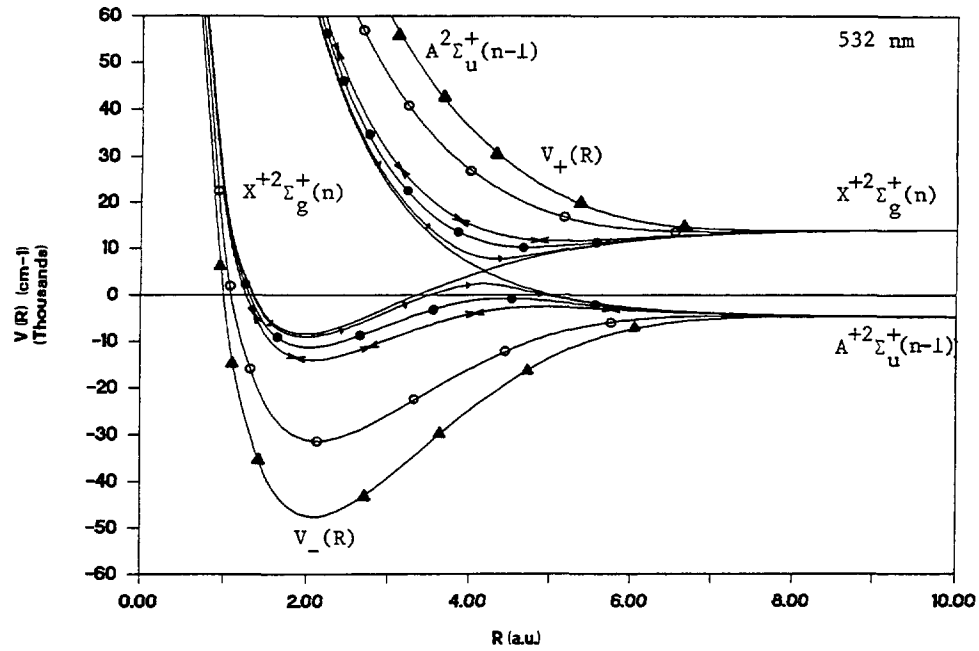

Fig. 3. — Laser-induced avoided crossing creating new dressed adiabatic potentials $V_+(R)$ and $V_-(R)$, equation (21) as a function of laser intensity I (W/cm^2) 0 (——) ; 10^{12} (,,,) , 5×10^{12} (···) , 10^{13} (×××) ; 5×10^{13} (OOO) ; 10^{14} (▲▲▲)

nonresonant two photon dissociation of the electronic ground state of H_2^+ *via* the nonresonant repulsive A^+ $(n-3)$ state. Thus the A^+ $(n-3)$ serves as a *virtual* state, i.e , the dissociation products remain on the X^+ potential, but the radiative transition is induced by the A^+ repulsive potential which is nonresonant, and is therefore inaccessible. This is clearly seen in figure 2 where the A^+ $(n-3)$ state is always well above the X^+ $(n-4)$ channel Thus only resonant processes give rise to crossing potentials, whereas nonresonant processes always have well separated potential surfaces This two photon nonresonant transition from bound X^+ nuclear states to continuum X^+ nuclear states has been called by us previously ATPD (above threshold photodissociation) and is the analogue of ATI [7, 26]. The conditions for such processes is large transition dipole moments as in ATI where the ion-electron system give a dipole moment equal to the distance r between the two. In ionic molecules such as LiF, the dipole moment of the system is R, i e. the distance between the ionic moities Li^+ and F^-. Thus a linearly diverging dipole moment arises, creating a very strong coupling with the radiative field as in the ATI case For the $X^+ \rightarrow A^+$ transition, we will show below that the transition dipole moment is $R/2$, i e half the internuclear distance Thus in all three cases, similar nonlinear absorption phenomena occur because of the large dipole or transition moments which give rise to very large radiative couplings as the ionized or dissociated species separate.

As in the ATPD of H_2^+ described above, ATPD of H_2 also occurs in the B state of H_2 Thus from figure 2 one has also an open channel the $B(n-2)$ channel accompanied by the EK, $GF(n-3)$ state, which are coupled radiatively with the B state also with an $R/2$ transition moment. Thus neutral $H(1s) + H(n=2)$ atoms are expected to be also created due to ATPD in the neutral B, EK, GF states of H_2. In the next section we will try to render these

predictions quantitative as a result of the numerical efficiency of the coupled equations (9)-(10) which enable one to include as many channels as are deemed necessary by convergence criteria. Furthermore, as emphasized above, one can readily cover the weak field, perturbative regime, $I \sim 10^{10}$ W/cm^2 to the high field nonperturbative limit $I \sim 10^{14}$ W/cm^2, and include simultaneously bound-bound, bound-continuum, radiative and nonradiative transitions in one unified formalism and numerical method.

4. Results and discussion.

As discussed in the previous sections, collision theory allows one to obtain, using the artificial channel $|C1\rangle$, transition amplitudes from initial bound states to final bound states or continua In our case, we shall be calculating the transition amplitudes from the $v = 0$ vibrational state of the ground electronic state $X\ ^1\Sigma_g^+$ of H_2 to the various channels that are open according to the field-molecule diagram, figure 2, i.e. all the channels which are below the zero energy line which corresponds to the initial energy.

The input in the coupled equations (9) are the *ab-initio* potentials of H_2 and H_2^+ published in the literature [39, 40]. These were interpolated over 3 000 points over an internuclear distance of 0.4 to 33 a.u. In the case of the EF and GK states, since these are calculated *adiabatically* [41], these well known double well potentials were deperturbed [12, 33], in order to produce the crossing *diabatic* potentials GF and EK A gaussian *nondiabatic* nonradiative interaction V_{12}^m was found of the form $V_{12}(R) = 3\,023\ (\text{cm}^{-1}) \exp[-38.2\ (R - 0.29)^2]$ to give the above cited adiabatic potentials EF and GK when the nondiabatic matrix (without $\hbar\omega$) is diagonalised (Eqs (20)-(21)).

As to the radiative couplings, two equivalent gauges are possible [5, 6, 25], the electric-field (multipole) gauge or the radiation field (Coulomb) gauge. The radiative coupling in the first is $e\mathbf{r} \cdot \boldsymbol{\mathcal{E}}$ whereas in the last it is $e\mathbf{A}/mc \cdot \mathbf{p}$. (In the latter, the A^2 term can be eliminated by a unitary transformation for all levels and is therefore of non consequence [5, 6]) Both gauges will give identical results if a complete set of states is used, since the two gauges are related by a unitary transformation. The use of one gauge or another thus depends on its convenience. In the present problem, the electronic transitions $B \rightarrow F$ and $X^+ \rightarrow A^+$ involve excitation to electronic states which have the same asymptotic limits. In fact the $B \rightarrow F$ and $X^+ \rightarrow A^+$ transitions are both $1s\sigma_g \rightarrow 2p\sigma_u$ molecular orbital transitions [9]. For these, the transition moment is easily shown to be [15]

$$\boldsymbol{\mu}(R) = \left\langle \frac{1s_a + 1s_b}{\sqrt{2}} \,|\, e\mathbf{r} \,|\, \frac{1s_a - 1s_b}{\sqrt{2}} \right\rangle = eR/2\,, \tag{23}$$

in the limit of nonoverlapping atomic orbitals $1s_a$ and $1s_b$. Clearly in the asymptotic atomic limit, these moments become infinite, implying very strong coupling of the molecule to the electromagnetic field upon dissociation. Unfortunately this creates divergent radiative couplings in the electric field gauge It is therefore best to use the Coulomb gauge, which as the result of the commutation relation $\hat{p}/m \equiv (i/\hbar)[\hat{H}, r]$, results in the following convergent radiative coupling .

$$\frac{\mathbf{A}}{mc} \cdot \mathbf{p}_{ij} = \frac{(V_i(R) - V_j(R))}{\hbar\omega}\, \mathbf{R}/2 \cdot \boldsymbol{\mathcal{E}}\,, \tag{24}$$

where V_i and V_j are electronic potentials and we have used the relation $\boldsymbol{\mathcal{E}} = -\frac{1}{c}\frac{\partial \mathbf{A}}{\partial t}$. Thus as $R \rightarrow \infty$, $V_i(R) - V_j(R) \rightarrow 0$ and the expression (23) converges to zero. The Coulomb gauge

transition moment (23) was therefore used in the radiative transition calculations for the transitions B → F and $X^+ \rightarrow A^+$ (a calculation for H_2^+ with the Coulomb gauge (23) has been recently reported by Atabek *et al* [41]). The X → B five photon transition was simulated by using an arbitrary weak effective one photon transition, which is of no consequence since this transition is perturbative. Finally the E and G to X^+ transitions being unknown were given the arbitrary transition moment $\mu = 1\ \text{cm}^{-1}$. Other transition moments such as B → E, G were taken from the literature [43].

Calculations were performed for the transition amplitudes T_{0C}, equation (20) for the open channels below the initial zero energy, corresponding to the $v = 0$ level of $X\ ^1\Sigma_g^+$ (see Fig. 2). Since the seventh photon falls in energy just above the $v = 3$ level of X^+ ($^2\Sigma_g^+$), then the $v = 0$ to 3 vibrational levels of X^+ $(n-2)$ all lie below this zero energy line (Fig. 2). It is to be emphasized that this figure corresponds to zero kinetic energy of the electron. In actual fact, in the photoionization process $H_2 \rightarrow H_2^+ + e^-$, the electron acquires considerable kinetic energy which is then analyzed, thus exhibiting ATI peaks [9-10]. Since we are interested in the dressing of the molecular ion H_2^+, we can obtain the energies and photodissociation widths of the vibrational levels of H_2^+ in the presence of the laser field by examining the resonance structure of T_{0C}. In fact, these resonances show up in numerical calculations of T_{0C} when one scans as a function of energy the levels of H_2^+ in anyone open channel, from $A^+(n-3)$, $B(n-2)$, EF, gK$(n-3)$, $X^+(n-4)$ to $A^+(n-5)$. One takes into account the electronic kinetic energy by shifting up all the H_2^+ channels, i.e. X^+ and A^+. As one calculates T_{0C} as a function of this displacement of the H_2^+ channels (we reiterate this corresponds to calculating T_{0C} as a function of electron kinetic energy), one finds that resonances appear corresponding to $v = 3, 2, 1, 0$ successively from low to high electron kinetic energy. This is as expected, since at low electron kinetic energy, the molecule remains in its high vibrational states, whereas at high electron kinetic energy, only low vibrational excitation can remain by conservation of total energy. These resonances (normalized to unity by dividing by the maximum value of the resonance) show a Lorentzian behaviour for $I < 10^{13}\ \text{W/cm}^2$ and non-Lorentzian behaviour for $I \geqslant 10^{13}\ \text{W/cm}^2$. Thus for the first case, a linewidth can be readily obtained from the half-width at the middle of the resonance curve, whereas in the other cases, the average of the two half-widths at the middle was used as a first order approximation We emphasize that the same resonances appear in all the open channels, thus confirming that the energy shifts and widths correspond to all possible photophysical processes included in the calculation as illustrated in the field-molecule representation (Fig. 2) which goes well beyond the perturbative description depicted in figure 1

The effect of avoided crossings on proton yields is summarized in table I where we tabulate the peak intensities of the laser induced resonances which should appear as peaks in the kinetic energy distribution of the protons produced in the channels discussed above. The peak intensities reflect the tenth-order Franck-Condon distributions in the ten-photon process depicted in figure 1 At intensities below $I < 10^{11}\ \text{W/cm}^2$, the relative peak heights for different laser intensities $I(\text{W/cm}^2)$ was found to follow the expected perturbative I^n law, where n is the number of photons observed in an n-th order process. Above $I = 10^{11}\ \text{W/cm}^2$, such a law is no longer followed according to table I As an example, the $B(n) \rightarrow A^+(n-5)$ transition should scale as I^5. One observes in fact a maximum in the resonance peaks at $10^{12}\ \text{W(cm}^2)$ and a decrease at $10^{13}\ \text{W/cm}^2$ in the $A^+(n-5)$ channel. The $X^+(n-4)$ channel exhibits an unusual increase in probability with respect to the $A^+(n-5)$ channel between $I = 10^{12}$ and $10^{13}\ \text{W/cm}^2$. The most logical explanation for this reversal in yield in the $X^+(n-4)$ and $A^+(n-5)$ channel is the laser induced avoided

Table I. — *Peak intensities of laser-induced resonances* (v) *for different open channels* (Fig. 2) *as a function of intensity* I (W/cm^2)

I/v		$A^+(n-3)$	$B(n-2)$	$X^+(n-4)$	$EK(n-3)$	$A^+(n-5)$
10^{11}	3	1×10^{-5}	$3\,6 \times 10^{-3}$	10^{-6}	1.5×10^{-4}	2×10^{-5}
	2	9×10^{-6}	4×10^{-3}	8×10^{-4}	1.4×10^{-4}	9×10^{-3}
	1	—	4.5×10^{-3}	4×10^{-1}	$2\,1 \times 10^{-4}$	4
	0	—	3.6×10^{-3}	4×10^{-6}	$1\,4 \times 10^{-4}$	4×10^{-5}
10^{12}	4	2	9×10^{-3}	4×10^{2}	10^{-2}	3×10^{2}
	3	10^{-5}	8×10^{-3}	3.5	3×10^{-3}	2.5
	2	4×10^{-8}	8×10^{-3}	2×10^{-1}	3×10^{-3}	1.5×10^{-1}
	1	—	9×10^{-3}	10^{3}	3×10^{-3}	7×10^{2}
	0	—	9×10^{-3}	15	3×10^{-3}	10^{1}
10^{13}	7	3×10^{2}	0.7	10^{2}	0 5	4×10^{-1}
	6	3×10^{-2}	0.6	3×10^{1}	0 5	10^{-1}
	5	7×10^{-2}	0.6	3	0.5	10^{-2}
	4	—	0.7	2×10^{2}	0.5	4×10^{-2}
10^{14}	31	10^{5}	7×10^{2}	2×10^{2}	10^{3}	2×10^{-1}
	27	—	3×10^{-3}	10^{6}	2×10^{3}	4×10^{1}
	25	—	3×10^{5}	6×10^{6}	2×10^{5}	7×10^{2}

crossing which will occur according to figure 3 Thus since the transition moment $\langle X^+ \mid \mu \mid A^+ \rangle = R/2 \simeq 2.2$ a u. at the crossing, the radiative interaction (Rabi frequency ω_R, Eq. (4)) at $I = 10^{12}$ W/cm^2 is approximately 4 000 cm^{-1}, inducing a separation between V_+ and V_- adiabatic potentials of $2\,\omega_R = 8\,000$ cm^{-1} (see Fig. 3) This avoided crossing will therefore favour dissociation into the $X^+(n-4)$ channel over the $A^+(n-5)$, since according to the Landau-Zener formula of nonadiabatic transitions, increasing avoided crossings render these crossings more adiabatic [12, 15, 16, 34]. This reversal of proton yield, i.e., increase in lower kinetic energy protons with increasing laser intensity, has been observed by Bucksbaum and therefore confirms that the laser-induced avoided crossing mechanism becomes operative at intensities above 10^{12} W/cm^2 [10-11]

Our calculations show *new* interesting results Firstly, the lowest kinetic energy protons yield produced in the $A^+(n-3)$ channel by tunnelling from the $X^+(n-2)$ bound states into $A^+(n-3)$ as a result of the laser induced avoided crossings dominates above intensities $I = 10^{13}$ W/cm^2. This has not yet been observed experimentally and is again indicative of the laser-induced avoided crossing mechanism (Fig 3) Secondly, ATPD appears in the two channels : $B(n-2)$ and $X^+(n-4)$. The first corresponds to ATPD in the $B\,^2\Sigma_u^+$ state of H_2 producing neutral atoms which presumably will ionize in the laser field and contribute to the proton yield. Since in the previous section we pointed out that the transition moments in the $B \rightarrow F$ transition in H_2 and $X^+ \rightarrow A^+$ transition in H_2^+, both have the value $R/2$, it is not surprising that this process occurs in the neutral and ionized molecule. Due to the nondiabatic coupling between the F and G, E Rydberg states of H_2, ATPD in the B state has an anomalous intensity dependence From table I, one sees clearly that the radiative $B \rightarrow F$ coupling overwhelms the nondiabatic coupling so that above 10^3 W/cm^2, ATPD in the B state of H_2 becomes comparable to that of H_2^+, i.e., the $X^+(n-4)$ channel. As explained

in the previous section, this channel is the result of two-photon absorption, i.e., ATPD, in the X^+ electronic state, mediated by the nonresonant $A^+(n-3)$ state At intensities $I > 10^{12}$ W/cm^2, ATPD in H_2^+ exceeds the three photon dissociation of H_2^+ into the $A^+(n-5)$ channel. This is due to the laser induced avoided crossing, as explained above, between the $X^+(n-5)$ and $A^+(n-5)$ channel. We conclude therefore that ATPD in the $B\,^1\Sigma_u^+$ state of H_2 and the $X\,^2\Sigma_g^+$ state of H_2^+ dominate over the final ten photon dissociation channel $A^+(n-5)$. Thus since in experiments one measures proton yield (H^+), one cannot attribute this solely to the ATPD of H_2^+, but rather ATPD in H_2 will also be an important factor at high intensities. In particular, one notices that the nonradiative, nondiabatic coupling between the F and EK state of H_2 also creates neutral atoms as a result of ATPD induced in the B state.

As described above, the laser induced avoided crossings at energies illustrated in figure 2 affects the proton and hydrogen atom yields at intensities above 10^{11} W/cm^2, as measured by the peak intensities of the laser induced resonances near the zero initial energy Thus for $I \leqslant 10^{11}$ W/cm^2, four of these resonances occur and can be assigned to $v = 0$-3 of H_2^+ At $I \geqslant 10^{12}$ W/cm^2, new resonances occur as the radiative coupling which is measured by the electronic Rabi frequency ω_R, equation (4), makes the H_2^+ well even deeper From table II, one reads $\omega_R = 822$, 2 574, 8 224 cm^{-1} respectively for intensities 10^{11}, 10^{12} and 10^{13} W/cm^2 at the radiative crossing point $R_c = 4.2$ a.u As a result, extra levels will occur at the higher intensities which can be assigned as levels of $V_-(R)$ (Tab. II)

New levels, which we now call *adiabatic* levels will also occur above the crossing point R_c, trapped by the new laser induced potential $V_+(R)$ (Fig 3 and Eq. (21)) [15, 16]. In order to quantify the presence of these new levels, we tabulate in table II the energies of all resonances which appear in the ten photon photodissociation ionization amplitude $\langle {}^1\Sigma_g^+(H_2), v = 0, n+5 \mid T \mid A\,^2\Sigma_u^+, c, n-5 \rangle$, as obtained by the coupled equations (These same resonances appear in the other open channels below the zero energy line (Fig 3).) The positions of these levels appears as one scans the above amplitude as a function of kinetic energy E of the continuum nuclear state $|c\rangle$, i.e., as a function of total proton kinetic energy (the actual measured kinetic energy is $E/2$, since the total energy is shared by the two dissociating protons [10, 11]) We emphasize that this scanning is equivalent to scanning the kinetic energy of the ionized electron i.e., low energy electrons leave high energy protons, and vice versa.

We use two notations for the identification of the laser induced resonances · v_d corresponding to diabatic or weak field levels, and v_{ad} for adiabatic or strong field levels. Thus at $I = 10^{11}$ W/cm^2, the vibrational spacing for levels at the bottom of the H_2^+ well and below the radiative crossing point R_c are separated by $\sim 2\,200$ cm^{-1}, the H_2^+ vibrational frequency. The radiative crossing point $R_c - 4.2$ a.u. between the $A^+(n-5)$ and $X^+(n-4)$ channel occurs at the energy $E_c = 33\,560$ cm^{-1} below the initial ($v = 0$, $^1\Sigma_g^+(H_2)$) state The dissociation limits of $X^+(n-4)$ and $A^+(n-5)$ occur at 23 320 cm^{-1} and 42 120 cm^{-1} respectively below the initial energy of the $v = 0$, H_2 level. Thus as one scans the kinetic energy E of the protons from 0 to 42 120 cm^{-1}, one sees the $v = 0$-3 levels of the $X^+(n-2)$ state (Fig. 3) appear first as resonances in the ten photon photodissociation-ionization amplitude. The levels $v = 2$ and 3 *reappear* also at higher kinetic energies (40 552, 38 610 cm^{-1}, in parentheses, in Tab I) as levels of $X^+(n-4)$ since these are situated just above the asymptotic limit of $A^+(n-5)$. The depth of the $X^+(n-4)$ well is at 46 962 cm^{-1} for zero field. Similarly at 10^{12} W/cm^2, the $v = 3$ and 4 levels appear at low kinetic energy (1 061 and 177 cm^{-1}) and again at high kinetic energies (39 554 and 37 772 cm^{-1}). The spacings and widths of these levels being identical at the two different kinetic energies is a

Table II. — *Proton kinetic energy* E (cm^{-1}) *and linewidths* Γ (cm^{-1}) *for laser induced resonances.* v_d *(diabatic) or* v_{ad} *(adiabatic) — as a function of intensity* I (W/cm^2); $\lambda = 532$ nm; ω_R (cm^{-1}) — *electronic Rabi frequency* (Eq. (4)) *at* $R_c = 4.2$ a.u., *radiative crossing point.*

I	10^{11} ($\omega_R = 822$)			10^{12} ($\omega_R = 2\,574$)			10^{13} ($\omega_R = 8\,224$)		
v_d	E	Γ	v_{ad}	E	Γ	v_{ad}	E	Γ	v_{ad}
0	7 204	0.003		8 080	4		13 630	4 5	
1	5 018	0.01		5 914	2		11 664	127	
2	2 958	0.005		3 875	4		9 796	498	
	(40 552)								
3	1 016	0.006		1 961	0.1		7 334	859	
	(38 610)			(39 554)					
4	36 788	0.11		177	1 2		5 658	0 1	
				(37 772)					
5	35 090	2.5		36 150	3		2 960	285	
6	33 534	25		34 786	156		1 631	135	
							(39 174)		
7	32 062	190		33 144	910		337 232	1 287	
8	30 548	270	0				34 344	1 621	
9	29 362	34	1				30 966	1 677	
10	28 142	65	2	28 728	22	0	27 800	1 514	
11	27 140	140	3	27 318	17	1	26 086	7×10^{-4}	0
12	26 256	67	4	26 126	88	2	25 228	3×10^{-3}	1
13	25 422	8	50	25 200	79	3	24 530	4×10^{-3}	2
14	24 744	0.5	6	24 478	42	4	23 992	5×10^{-3}	3
15	24 182	8	7	23 946	12	5	23 614	4×10^{-3}	4
16	23 760	10	8	23 584	3	6	23 398	$< 10^{-4}$	5
17	23 482	10	9	23 384	0.8	7	23 328	$< 10^{-4}$	6
18	23 348	4	10	23 326	0.2	8			
19	23 322	0.7	11						

proof of the convergence of the calculations. Since the depth of the $X^+(n-2)$ well is $\sim 8\,000$ cm^{-1} below the initial energy, only $v = 0$-3, 0-4 levels are seen at low energies. The bottom level $v = 0$ for $I = 10^{13}$ W/cm^2 occurs at $E = 13\,630$ cm^{-1} due to the depression of the well minimum by the radiative coupling, i.e., the electronic Rabi frequency ω_R.

Thus at low proton kinetic energies one observes the $X^+(n-2)$ vibrational levels below the initial zero energy. The next levels occur as soon as the asymptotic limit of the $X^+(n-4)$ potential reaches the zero initial energy. These next levels are now situated above the radiative crossing R_c between $X^+(n-4)$ and $A^+(n-5)$ which at high intensities develops into two new adiabatic surfaces $V_+(R)$ and $V_-(R)$, equation (21). Thus between 42 120 cm^{-1} (the asymptotic energy of $A^+(n-5)$) and 23 320 cm^{-1} (the asymptotic energy of $X^+(n-4)$) one should observe levels above and below the radiative crossing R_c. Following the diabatic assignment v_d for low intensities, $I = 10^{11}$ W/cm^2, one observes very broad levels around $E_c = 33\,560$ cm^{-1}, the crossing point energy at R_c. The minimum of

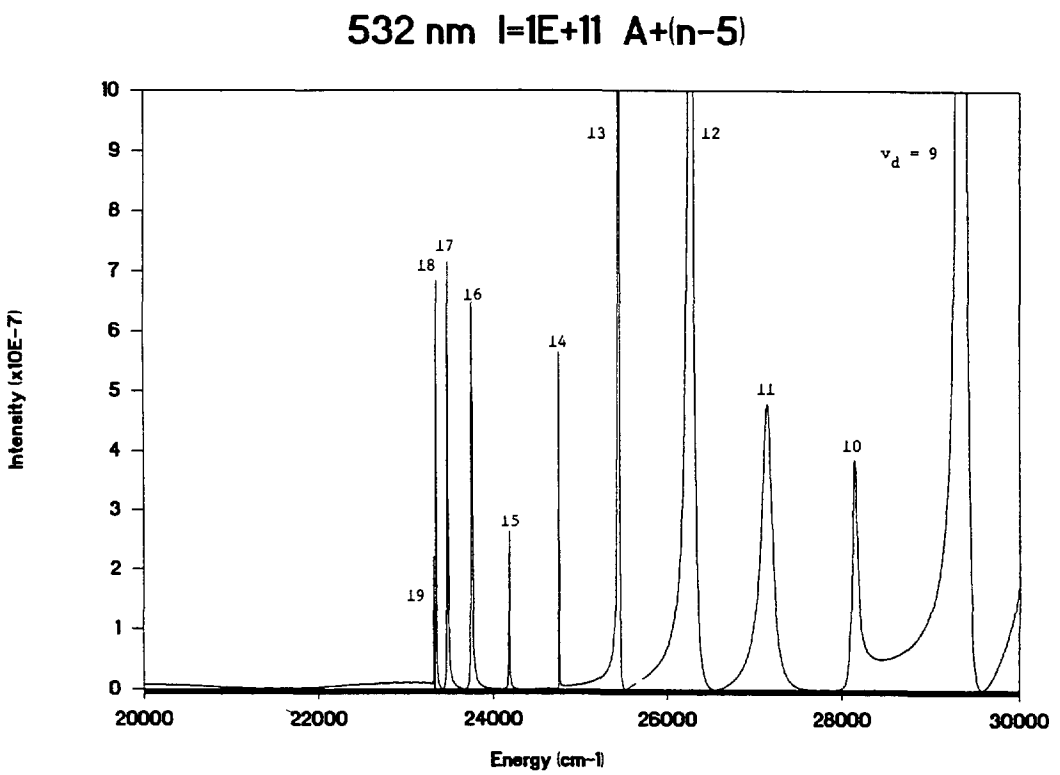

Fig 4 — Laser induced resonances as a function of proton kinetic energy E in the ten photon photodissociation-ionization probability of H_2 (Fig. 1). (Radiative crossing energy $E_c = 33\,560\ \text{cm}^{-1}$ for $\lambda = 532$ nm, Fig 3)

$V_+(R)$, i.e. $V_+(R_c)$ is situated at an energy ω_R above this crossing point energy E_c to which one must add the zero point energy of $V_+(R)$ in order to find approximately the position of the first adiabatic level $v_{ad} - 0$. These are listed in table II and therefore correspond to the levels above the radiative crossing point R_c which can be assigned to the $V_+(R)$ potential (see also Fig. 4).

In actual fact, the laser induced resonances are *diabatic* levels at low intensities, $\omega_R \ll \omega_v$, i.e., Rabi frequencies ω_R are less than zero field vibrational frequencies ω_v. At higher intensities, $\omega_R \sim \omega_v$, and the exact (dressed) levels can be considered to be linear combinations of diabatic levels (of $V(R)$) and adiabatic levels (of $V_\pm(R)$) [15, 16] At high intensities, where $\omega_R \gg \omega_v$, the real dressed levels above R_c converge to the *adiabatic* levels of $V_+(R)$ with increasing intensity. This effect can be clearly seen from table II, where at $I = 10^{13}\ \text{W/cm}^2$, levels between $26\,086\ \text{cm}^{-1}$ and the $X^+(n-4)$ asymptotic energy, $23\,320\ \text{cm}^{-1}$ have widths less than $0.1\ \text{cm}^{-1}$ (The level at $26\,086\ \text{cm}^{-1}$ was found to be the first adiabatic level, $v_{ad} = 0$, of $V_+(R)$ by an independent two channel calculation). The increasing stability of levels above the radiative crossing point R_c with increasing intensity I and thus increasing diabatic coupling $V_{ee'} = \omega_R$ (Eq (2)), is typical of curve crossing systems, with the new adiabatic levels becoming levels of the new adiabatic potential $V_+(R)$ [15, 16].

In figure 4 we show the relative intensities of the laser induced resonances between the radiative crossing energy $E_c = 33\,560\ \text{cm}^{-1}$ and the asymptotic limit, $23\,320\ \text{cm}^{-1}$ of the $X^+(n-4)$ potential, the latter corresponding to ATPD as discussed previously These

resonances show anomalous intensities, i e., the sharp levels near the dissociation limit at 23 320 cm^{-1} have lower peak intensities than the broad levels near the radiative crossing point These anomalies are clearly due to the highly nonlinear radiative transitions at high intensities. Thus levels near the radiative crossing have the largest radiative widths, table II, and simultaneously these have the largest peak intensities. Since these peak intensities reflect the total ten-photon dissociation-ionization probability of H_2 into H_2^+, and the widths of the peaks reflect the three-photon dissociation probability of H_2^+, no simple Franck-Condon picture is applicable due to the radiative induced avoided crossings [15, 16] Similar conclusions have been shown to apply in the interpretation of the ATI peaks observed, i.e. the vibronic peaks of H_2^+ in the nonlinear photoelectron spectrum of H_2 did not conform to usual Franck-Condon predictions [9]. Finally, these resonances show some nonsymmetrical behaviour (e.g. $V_a = 9, 12$). This reflects complex interferences in the ten photon amplitude T_{0C}, due to the many possible photon pathways illustrated in figure 2.

In conclusion, we have shown that laser induced crossings are operative in the high intensity photodissociation-ionization of H_2. In particular, these crossings enhance above threshold photodissociation-ATPD — in the B state of H_2 and the X state of H_2^+. We have also shown that laser-induced resonances appear clearly in the open channels, i.e. in all the accessible photodissociation channels of H_2^+ and H_2. In particular, at the high intensities, $I \geqslant 10^{13}$ W/cm^2 for which the adiabatic picture illustrated in figure 3 becomes operative due to the large Rabi frequency ω_R (1/2 the gap at R_c, the avoided crossing between V_+ and V_-), new adiabatic states of $V_+(R)$ become more stable with increasing intensity These new states have been identified recently in the ATI spectrum, i e., in the nonlinear photoelectron spectrum of H_2 [44] Our numerical results suggest that these new states should also appear as sharp resonances in the high kinetic energy spectrum of the proton yield.

In the present case we have neglected higher excited electronic states of H_2^+ and rotations. Since the $\Sigma_g^+ \rightarrow \Sigma_u^+$ has an R/2 transition moment, this clearly is the most important transition for H_2^+. As for rotations, our previous calculations [19, 27], show that efficient rotational excitation can occur leading to orientation of the molecule in the field. This may alter the narrow widths by making accessible more dissociating channels. However we have found in these previous calculations that narrow laser induced resonances will remain stable in the presence of rotational excitations [27].

Acknowledgments.

We thank the Natural Sciences and Engineering Research Council of Canada (NSERC) and the National Center of Excellence in Molecular Dynamics (CEMAID) for grants supporting this research. All calculations were performed on an IBM-RISC-6000-530 workstation. We also thank Miss D. Marchand for computer assistance.

References

[1] SLATER J C., Quantum Theory of Molecules and Solids, vol I (McGraw Hill, N Y., 1963)
[2] GALLAGHER J., BRION C E , SAMSON J A R and LANGHOFF P. W., *J Phys Chem Ref Data* **17** (1988) 9.
[3] BAWAGAN A D and BRION C. E , *Chem Phys Lett.* **137** (1987) 573
[4] DUKE C B., LIPARI N D and PIETRONERO L., *J Chem Phys* **65** (1976) 1165
[5] MITTLEMAN M. H , Introduction to the Theory of Laser — Atom Interactions (Plenum Press, N.Y , 1982)

[6] FAISAL F H M, Theory of Multiphoton Processes (Plenum Press, N Y, 1987)
[7] BANDRAUK A. D, Ed, Atomic and Molecular Processes with Short Intense Laser Pulses, vol. B-171, NATO ASI Series (Plenum Press, N Y, 1988)
[8] CORNAGGIA C, NORMAND D, MORELLEC J, MAINFRAY G. and MANUS C., *Phys Rev.* **A 34** (1986) 207
[9] VERSCHUUR J. W J, NOORDAM L. D. and VAN LINDEN VAN DEN HEUVELL H. B., *Phys. Rev* **A 40** (1989) 4383
[10] BUCKSBAUM P H., ZAVRIYEV A, MULLER H G and SCHUMACHER D W, *Phys Rev. Lett.* **64** (1990) 1883
[11] ZAVRIYEV A, BUCKSBAUM P H, MULLER H G. and SCHUMACHER D W., *Phys Rev.* **A 42** (1990) 5500
[12] LEFEBVRE-BRION H and FIELD R W, Perturbations in Spectra of Diatomic Molecules (Academic Press, Orlando, FL, 1986)
[13] CHELKOWSKI S. and BANDRAUK A. D, *J Chem Phys* **89** (1988) 3618
[14] CORKUM P B., BURNETT N H. and BRUNEL F, *Phys Rev Lett.* **62** (1989) 1259
[15] BANDRAUK A. D and SINK M L., *J Chem Phys* **74** (1981) 1110
[16] BANDRAUK A D and MCCANN J F., *Comm At Mol Phys* **22** (1989) 325
[17] SU Q and EERLY J H, *J Opt Soc Am* **B 7** (1990) 564
[18] SU Q, EBERLY J. H and JAVANAINEN J, *Phys. Rev. Lett.* **64** (1990) 862
[19] MCCANN J F and BANDRAUK A D, *Phys Rev* **A 42** (1990) 2806
[20] BANDRAUK A. D and GÉLINAS N, *J. Comp Chem* **8** (1987) 313
[21] COHEN-TANNOUDJI C. C., DUPONT-ROC J and GRYNBERG G, Photons and Atoms (J Wiley & Sons, N Y, 1990).
[22] NGUYEN-DANG T T and BANDRAUK A D, *J Chem Phys* **79** (1983) 3256
[23] GOLDIN E, Waves and Photons (J Wiley & Sons, N Y., 1982)
[24] GLAUBER R J., *Phys Rev* **131** (1963) 2766
[25] BANDRAUK A. D, KALMAN O and NGUYEN-DANG T T, *J Chem Phys* **84** (1986) 6761.
[26] BANDRAUK A. D and GAUTHIER J M., *J. Opt Soc Am* **B 7** (1990) 1420
[27] BANDRAUK A. D and TURCOTTE G, *J Phys Chem* **87** (1983) 5098
[28] NGUYEN-DANG T T., DUROCHER S and ATABEK O, *Chem Phys* **129** (1989) 452
[29] NORCROSS D W. and SEATON M J, *J Phys* **B 6** (1973) 614.
[30] HE X, ATABEK O and GUISTI-SUZOR A, *Phys Rev* **A 38** (1988) 5586
[31] SHAPIRO M., *J Chem. Phys* **56** (1972) 2582
[32] WATSON K M and NUTTAL J, Topics in Several Particle Dynamics (Holden Day Publishers, San Francisco, 1967)
[33] BANDRAUK A D, TURCOTTE G, *J Phys. Chem* **89** (1985) 3039.
[34] BANDRAUK A D and CHILD M S, *Mol Phys* **19** (1970) 95
[35] VORONIN A I and SAMOKHIN A. D., *JETP (Sov Phys)* **43** (1976) 4
[36] LAU A M and RHODES C K, *Phys. Rev* **A 16** (1977) 2392
[37] GEORGE T F and YUAN J. M, *J. Chem Phys* **68** (1978) 3040
[38] BANDRAUK A D. and SINK M. L, *Chem Phys Lett* **57** (1978) 569.
[39] KOLOS W, *Atomic Data* **2** (1971) 119
[40] WOLNIEWICZ L. and DRESSLER K, *J Chem Phys* **82** (1985) 3292
[41] WOLNIEWICZ L. and DRESSLER K, *J Molec Spectrosc* **77** (1979) 286
[42] HE X, ATABEK O and GUISTI-SUZOR A, *Phys Rev.* **A 42** (1990) 1585
[43] WOLNIEWICZ L., *J Chem Phys* **51** (1969) 5002.
[44] ALLENDORF S and SZOKE A, submitted to *Phys Rev A*; Livermore Report #UCRL-JC-104234